JBC Papers in Press. Published on December 2, 2015 as Manuscript M115.687632
The latest version is at http://www.jbc.org/cgi/doi/10.1074/jbc.M115.687632



# Visualization of $NO_3^-$/$NO_2^-$ Dynamics in Living cells by Fluorescence Resonance Energy Transfer (FRET) Imaging Employing a Rhizobial Two-Component Regulatory System.

**Masafumi Hidaka,[1,†] Aina Gotoh,[1,†] Taiki Shimizu,[1] Kiwamu Minamisawa,[2] Hiromi Imamura,[3] and Takafumi Uchida[1].**

[1] From the Department of Molecular Cell Science, Tohoku University, Sendai 981-8555, Japan; [2] Department of Environmental Life Sciences, Tohoku University, Sendai 980-8577, Japan; [3] The Hakubi Center for Advanced Research, Kyoto University, Kyoto 606-8501, Japan.

Running title; sNOOOpy, a sensor for nitrate/nitrite in living cells

To whom correspondence should be addressed: Takafumi Uchida, Molecular Enzymology, Department of Molecular Cell Science, Graduate School of Agricultural Science, Tohoku University, 1-1 Amamiya, Tsutsumidori, Aoba, Sendai, Miyagi 981-8555, Japan, Tel.: 81-22-717-8775; Fax 81-22-717-8778**;** E-mail: uchidat@biochem.tohoku.ac.jp

†, Both authors made equal contributions to the manuscript.

**Key words:** Fluorescence Resonance Energy Transfer (FRET), bacterial signal transduction, biosensor, protein-protein interaction, *in vivo* imaging, nitrogen metabolism, $NO_3^-$/$NO_2^-$ in physiology.

## ABSTRACT

Nitrate ($NO_3^-$) and nitrite ($NO_2^-$) are the physiological sources of nitric oxide (NO), a key biological messenger molecule. $NO_3^-$/$NO_2^-$ exerts a beneficial impact on NO homeostasis and its related cardiovascular functions. To visualize the physiological dynamics of $NO_3^-$/$NO_2^-$ for assessing the precise roles of these anions, we developed a genetically encoded intermolecular fluorescence resonance energy transfer (FRET)-based indicator, named sNOOOpy (sensor for $NO_3^-$/$NO_2^-$ in physiology), by employing $NO_3^-$/$NO_2^-$-induced dissociation of NasST involved in the denitrification system of rhizobia. The *in vitro* use of sNOOOpy shows high specificity for $NO_3^-$ and $NO_2^-$, and its FRET signal is changed in response to $NO_3^-$/$NO_2^-$ in the micromolar range. Furthermore, both an increase and decrease in cellular $NO_3^-$ concentration can be detected. sNOOOpy is very simple and potentially applicable to a wide variety of living cells and is expected to provide insights into $NO_3^-$/$NO_2^-$ dynamics in various organisms, including plants and animals.

Nitrate ($NO_3^-$) and nitrite ($NO_2^-$) are metabolites in the biological nitrogen cycle. In bacteria and plants, $NO_3^-$ is used as a substrate for respiration and/or assimilation. In animals, including humans, $NO_3^-$ and $NO_2^-$ ($NO_3^-$/$NO_2^-$) were recognized for a long time as being merely

inert oxidants of nitric oxide (NO) (1). NO is a key signaling molecule that regulates a vast range of physiological functions, such as vascular homeostasis, neurotransmission, and host defense (2). Intriguingly, many studies over the last decade revealed that these inert $NO_3^-/NO_2^-$ are physiologically recycled to form NO and other reactive nitrogen species through the "nitrate-nitrite-nitric oxide ($NO_3^-$-$NO_2^-$-NO) pathway" (3–5). Currently, $NO_3^-/NO_2^-$ are considered as stable reservoirs for NO-like bioactivity, and several beneficial aspects of $NO_3^-/NO_2^-$ in the treatment and prevention of cardiovascular diseases by restoring NO homeostasis are reported (5, 6).

As the regulation of $NO_3^-/NO_2^-$ in physiological processes is an attractive therapeutic target, it is important to understand $NO_3^-/NO_2^-$ in biological processes, how intracellular levels are regulated and how they control cellular processes. The most frequently used method for $NO_3^-/NO_2^-$ measurement is based on the Griess reaction (7). The Griess method is also used to assess NO synthesis because of the immediate conversion of NO into $NO_3^-/NO_2^-$ (half-life 2-6 s) (8). Although measurement of $NO_3^-/NO_2^-$ by the Griess assay is simple and convenient, it is difficult to apply this method for *in situ* measurement in living cells because this method is generally used as end-point assay that involves several chemical reactions. As for mammalian cells, although $NO_3^-$ influx into HeLa-derived cells at low pH condition was observed by patch-clamp method (9), detections of the dynamics of $NO_3^-/NO_2^-$ in physiological processes are quite difficult by presently available methods.

In some microorganisms, *nasST* genes are clustered together with other genes involved in $NO_3^-$ assimilation (10–13). NasS and NasT are annotated as a $NO_3^-/NO_2^-$-responsive two-component system, where NasS is a $NO_3^-/NO_2^-$ sensor, and NasT, a transcription antiterminator. We have previously demonstrated that the NasS and NasT from the root nodule bacterium *Bradyhizobium japonicum* form a stable complex (NasST) in the absence of $NO_3^-/NO_2^-$, and the formation of the NasS with $NO_3^-$ or $NO_2^-$ complex triggers release of the positive RNA-binding regulator NasT (13), which enhances the translation of proteins involved in $NO_3^-$ assimilation (Fig. 1A) (11). Herein, we report genetically-encoded FRET-based $NO_3^-/NO_2^-$ biosensors that employ NasS and NasT (Fig. 1B). Using this system, we succeeded in monitoring the dynamics of $NO_3^-/NO_2^-$ inside single living cells specifically.

## Experimental Procedures

*Gene construction*–The polymerase chain reaction (PCR) was performed with KOD-Plus Neo polymerase (Toyobo, Japan), and all of the oligonucleotide primers used in this study are listed in Table 1. DNA fragment assembly was performed using the In-Fusion HD Cloning Kit (Takara Bio, Japan). The *NasS* and *NasT* genes were amplified by PCR from a pUC-based clone library of *B. japonicum* (14). The cDNA of seCFP, YFP (Venus) variants with circular permutation (15) and the pCold I vector (Takara Bio) were amplified by PCR. The amplified genes were assembled to obtain pCold_CFP, pCold_CFP-NasT and pCold_NasS-YFP for expression in *Escherichia coli*. CFP and CFP-NasT were expressed as N-terminal $(His)_6$-tagged constructs, while NasS-YFP had a

$(His)_6$-tag added at its C-terminus. PCR-based mutagenesis and Quikchange (Stratagene) were used to construct mutants of seCFP (A206K) and NasS (H145A), respectively. The genes *CFP-NasT* and *NasS-Venus(cp195)* were cloned into a pFLAG-CMV-1 vector (Sigma-Aldrich) to obtain pCMV_sNOOOpy, which was used for mammalian expression. In pCMV_sNOOOpy, the FLAG sequence was replaced by the nuclear export signal sequence of HIV Rev (LPPLERLTL), and the genes *CFP-NasT* and *NasS-Venus_cp195* were arranged in tandem by self-processing 2A peptides.

*Purification of proteins*–The proteins CFP, CFP-NasT, NasS-YFP, GST-tagged NasT, and His-tagged NasS were expressed and purified from *E. coli* following the same procedures as described previously (13). Appropriate fractions were dialyzed against 10 mM HEPES pH 8.0. The homogeneity of purified proteins were established by SDS-PAGE analysis. The protein concentrations were determined using $A_{435}$ and molar extinction coefficient of 32,500 $M^{-1}cm^{-1}$ for CFP and CFP-NasT (16) and using $A_{515}$ and a molar extinction coefficient of 84,000 $M^{-1}cm^{-1}$ for NasS-YFP (17). The protein concentrations of GST-tagged NasT and His-tagged NasS were determined by the BCA Protein Assay kit (Pierce) using bovine serum albumin as a standard.

*Characterization of the sNOOOpy system*–The fluorescence of the sNOOOpy system was investigated in 100 mM HEPES pH 8.0 and 10 mM KCl using an FP-8200 spectrofluorometer (Jasco) at 25 °C. To obtain the fluorescence spectra, CFP was excited with 410 ± 10 nm light, and emission from 450 to 600 nm was scanned. The NasS-NasT binding assay was performed by using multi-well plates on a TECAN Spark 10M (excitation filter: 405 ± 10 nm, emission filter: 535 ± 10 nm). Emission with various concentrations of NasS-YFP or CFP-NasT were measured as described for the SUMO1 and Ubc9 interaction (18), with some modifications. The FRET emission was fitted using Kaleidagraph (Synergy software) with a single-site binding model.

Titration analyses were performed by FRET/CFP ratios against $[NO_3^-]$ or $[NO_2^-]$ (square brackets denote concentration of proteins/ligands). Plots were fitted with the following equations:

$$R = R_{\Delta\mathrm{NasT}} + (R_0 - R_{\Delta\mathrm{NasT}}) \times \frac{{K_\mathrm{D}}^n}{{K_\mathrm{D}}^\mathrm{n} + [\mathrm{NO_3^-}]^n}$$

where $n$ is the Hill coefficient, $K_D$ is a $[NO_3^-]$ or $[NO_2^-]$ dissociating half of NasST, $R$ = FRET/CFP ratio, $R_0$ = initial FRET/CFP ratio in the anion-free condition and $R_{\Delta NasT}$ = FRET/CFP ratio of NasS-YFP with CFP, respectively.

*Cell culture and microsocopy*–HeLa cells were obtained from Dr. Takeharu Nagai (Osaka University, Japan) and were cultured in DMEM (Nacalai, Japan) containing 5.5 mM glucose supplemented with 10% fetal bovine serum (Sigma). Cells were transfected with pCMV-sNOOOpy using Lipofectamine 2000 (Life Technologies). Then, cells were transferred to a glass-bottom dish (0.17-mm thickness, MatTek) coated with type I-C collagen (Nitta Gelatin, Japan). Cells cultured in phenol red-free DMEM were subject to imaging experiments 40-72 h after transfection.

The cells were maintained on a Ti-E inverted microscope (Nikon Corp., Japan) at 37 °C in a humidified atmosphere containing 5% $CO_2$

using a stage-top incubator (Tokai Hit, Japan) and were visualized through a Plan Apo 40×, 0.95 numerical aperture, dry objective lens (Nikon). The filters used for dual-emission ratio imaging of sNOOOpy were purchased from Semrock (Rochester, NY) and included an FF01-438/24 excitation filter, an FF458-Di02 dichroic mirror and two emission filters (an FF01-483/32 for CFP and an FF01-542/27 for YFP). Cells were illuminated using a xenon lamp through 25% and 12.5% neutral density filters. Fluorescence emissions from sNOOOpy were imaged using a scientific CMOS camera (Zyla 4.2, Andor Technologies). CFP and YFP images were obtained by alternating the emission filters with a filter exchanger. The exposure times were 200 ms for CFP and YFP images. The microscope system was controlled by NIS-Elements software (Nikon). Image analysis was performed using MetaMorph software (Molecular Devices). The YFP/CFP emission ratios were calculated by dividing YFP intensity by CFP intensity within a region of interest in a cell.

**RESULTS**

*Construction of a $NO_3^-$/$NO_2^-$ biosensor, sNOOOpy*–We invented an intermolecular FRET-based $NO_3^-$/$NO_2^-$ biosensor composed of a pair of two proteins: seCFP (19) linked with the N-terminus of NasT and YFP (Venus) (20, 21) fused with the C-terminus of NasS (Fig. 1C). As a preliminary step in the development, we attempted to find the best combination of the two classes of fluorescent proteins fused with NasT and NasS to improve the dynamic range and signal intensity. Among the combinations summarized in Fig. 1D, the FRET signal of the protein pair composed of CFP-NasT and NasS-Venus_cp195 (a circularly permutated Venus having the 195th amino acid as its N-terminus (15)) showed the highest increase in the formation of the NasS-NasT complex (NasST) and the largest change from the addition of $NO_3^-$. Therefore, this protein pair was subjected to characterization and further development.

When 1 μM CFP-NasT was mixed with 1 μM NasS-YFP, the FRET/CFP emission ratio increased to 1.8 as assessed by the emission ratio of 527/475 nm, a 3.6-fold increase from the CFP and NasS-YFP protein pairs (Fig. 1E and 1F, left panels). Additions of $NO_3^-$ and $NO_2^-$ abrogated the increase in the emission in a concentration dependent manner, while these anions showed no effects on emissions of fluorescence proteins (Fig. 1E and 1F). The change in FRET signal exhibited a high selectivity for $NO_3^-$ and $NO_2^-$. Among nine oxoanions summarized in Fig. 2, only $NO_3^-$ and $NO_2^-$ reduced the FRET ratio. Furthermore, such reductions induced by $NO_3^-$ were not interrupted by the presence of the other oxoanions. Thus, the indicator system can specifically detect the change in $NO_3^-$ and $NO_2^-$ levels as the FRET signal changes, which is caused by association and dissociation of NasS-YFP and CFP-NasT as designed in Fig. 1B. We termed the generated indicator system composed of CFP-NasT and NasS-YFP as sNOOOpy (sensor for $NO_3^-$/$NO_2^-$ in physiology). sNOOOpy-cp195, composed of CFP-NasT and NasS-Venus_cp195, was adopted as the wild-type sNOOOpy ($sNOOOpy^{WT}$), and the sNOOOpy variants constructed in this study are summarized in Table 2.

*In vitro characterizations of NasS-NasT interaction by sNOOOpy* –First, we characterized the protein interaction between CFP-NasT and NasS-YFP. Titration of 1 μM CFP-NasT with NasS-YFP showed that apparent dissociation constant ($K_{ST}$) between CFP-NasT and NasS-YFP is estimated to be 0.13 μM (Fig. 3A and 3B). The FRET ratio of sNOOOpy was decreased by titrate in increasing unlabeled [NasS], indicating that the interaction between NasS and NasT is reversible (Fig. 3C).

Next, we focused on $NO_3^-/NO_2^-$ sensing mechanism of NasST at molecular level. In rhizobial cell function, $NO_3^-/NO_2^-$ induce dissociation of NasST by binding to NasS. Therefore, we inferred that $NO_3^-/NO_2^-$ can be regarded as competitive inhibitor that compete with NasT for binding to NasS (Fig. 3D). Fig. 3E and 3F show titration of 1 μM NasS-YFP with CFP-NasT in the presence of various [$NO_3^-$]. Although curve-fitting analyses based on single-site binding model were failed because of the progressive decrease of FRET emission at high [CFP-NasT], the inhibitory effects of $NO_3^-$ at each [CFP-NasT] were comparable (Fig. 3G). $NO_3^-$ decreased FRET emission at low [CFP-NasT], while those at high [CFP-NasT] were recovered to the levels of $NO_3^-$-free conditions. These results supported that $NO_3^-/NO_2^-$ inhibit NasS-NasT formation competitively.

*Sensitivity of the sNOOOpy system in vitro* – Prior to further characterizations, we have prepared sNOOOpy$^{H145A}$, which is comprised of a NasS(H145A) mutant that was inferred to form a $NO_3^-$ binding site based on the $NO_3^-$ binding site structure of $NO_3^-$ binding protein NrtA (Fig. 4A) (22). Next, we characterized the sensitivity of the sNOOOpy system. In this study, we used $K_D$ values, the values at which the [$NO_3^-$] or [$NO_2^-$] dissociates half of the NasST, as the sensitivity determinant of the sNOOOpy system. Since the $K_D$ value corresponds to the half maximal inhibition concentration ($IC_{50}$) inhibiting a NasST formation in the competitive model as shown in the Fig. 3D, the $K_D$ values were determined by curve-fitting analyses using the Hill equation. Fig. 4B shows the FRET/CFP ratio from titration with $NO_3^-$ and $NO_2^-$. When 1 μM each of CFP-NasT and NasS-YFP was used, a micromolar [$NO_3^-$] decreased the FRET ratio, which is in good agreement with the affinity reported for NasST from *Paracoccus denitrificans* ($K_D \approx 15$ μM) (11). Under our *in vitro* assay conditions, the $K_D$ values for $NO_3^-$ and $NO_2^-$were estimated to be 39.5 μM and 256 μM, respectively. The FRET signal of sNOOOpy$^{H145A}$ was not reduced upon the addition of < 10 mM of $NO_3^-/NO_2^-$, indicating that NasS(H145A)-YFP and CFP-NasT form an extremely stable complex and lost $NO_3^-/NO_2^-$ responsiveness.

Elevated $K_D$ values corresponding to an increase in the [CFP-NasT] were observed (Fig. 4C). This characteristic in the sensitivities reflects that sNOOOpy is based on an intramolecular FRET system, where CFP-NasT and $NO_3^-$ competitively binds to NasS-YFP as shown in Fig. 3D. In a canonical competitive model, $IC_{50}$ values depend on the substrate concentration: $IC_{50} = (1 + [S]/K_m)K_i$, where $IC_{50}$, S, $K_m$, and $K_i$ correspond to $K_D$, CFP-NasT, $K_{ST}$, and $K_{S\text{-}NO3}$ in Fig. 3D, respectively. From the linear fit based on the equation, $K_{S\text{-}NO3}$ and $K_{S\text{-}NO3}/K_{ST}$ were calculated to be 6.0 μM and 39,

respectively (Fig. 4D). Estimated $K_{ST}$ value, 0.15 μM, was in good agreement with the value determined by titration of CFP-NasT with NasS-YFP, 0.13 μM, as shown in Fig. 3B.

The time course of FRET ratio changes at 20 – 100 μM $NO_3^-$ revealed that the rates of $NO_3^-$ binding ($k_{on}$) and dissociation ($k_{off}$) were determined based on the first order fitting to be $2.3 \times 10^{-3}$ $\mu M^{-1}s^{-1}$ and 0.10 $s^{-1}$, respectively (Fig. 5A and 5B). Thus, sNOOOpy system can detect [$NO_3^-$] changes on a time scale of seconds.

The fluorescence emission ratio was almost invariant from pH 7.0 to 8.5 and over a temperature range of 25 to 40 °C, suggesting that the sensitivity of sNOOOpy will not be affected by small fluctuations in pH and temperature (Fig. 5C and 5D). The $K_D$ value for $NO_3^-$ at 37 °C (37.9 μM) is almost identical to that at 25 °C (39.5 μM) (Fig. 5E). Thus, these results showed that we can quantify [$NO_3^-$] in a range of 1 – 1000 μM by sNOOOpy under standard *in vitro* assay conditions.

*Imaging of $NO_3^-$/$NO_2^-$ levels inside single living cells*–Next, we visualized the $NO_3^-$/$NO_2^-$ levels inside of a single living HeLa cell expressing sNOOOpy proteins. First, we constructed a mammalian expression plasmid for sNOOOpy, pCMV-sNOOOpy (Fig. 6A), in which cDNAs coding for CFP-NasT, a self-processing 2A-peptide and NasS-YFP were arranged in tandem (23, 24). A single polypeptide of CFP-NasT-2A-NasS-YFP is expected to be cleaved at the 2A site. As a result, CFP-NasT and NasS-YFP were separately expressed (Fig. 6B), which is parallel to the *in vitro* assay conditions. In addition, a nuclear exporting signal sequence was added to the N-terminus of CFP-NasT to prevent importation of the liberated CFP-NasT into the nucleus. sNOOOpy proteins expressed by pCMV-sNOOOpy were properly localized to the cytoplasm and exhibited a high FRET/CFP ratio (1.0 – 1.6) in the $NO_3^-$/$NO_2^-$-free medium, indicating the formation of the dimer of CFP-NasT and NasS-YFP (Fig. 6C). The FRET/CFP ratios were reduced in response to an increase in [$NO_3^-$] (Fig. 6C – E, and Supplementary Movie 1).

In the HeLa cells expressing sNOOOpy$^{WT}$, although up to 0.1 mM $NO_3^-$ induced no obvious changes of FRET/CFP ratio (Fig. 6D), $NO_3^-$ at a concentration of 0.3 mM induced a significant and rapid decrease in the FRET/CFP ratio, and the ratio was decreased about 50% by addiotion of 3 mM $NO_3^-$ (Fig. 6E). The HeLa cells containing sNOOOpy$^{WT}$ were less sensitive to $NO_2^-$ compared with $NO_3^-$, but apparent changes in the FRET/CFP ratio were detectable at 1 mM of $NO_2^-$ (Fig 6C middle panel). The HeLa cells with sNOOOpy$^{H145A}$, which formed stable NasST complexes and lost $NO_3^-$/$NO_2^-$ responsiveness, were insensitive to a change in ambient [$NO_3^-$] (Fig. 6C bottom panel). It should be noted that the response of sNOOOpy to $NO_3^-$ is reversible. Fig. 7, and Supplementary Movie 2 show the time course of the FRET/CFP ratio when the medium [$NO_3^-$] was alternately changed. The FRET/CFP ratio was reduced from 1.4 to 0.8 (40% decrease relative to that in 0 mM) when the cells were cultured in DMEM medium containing 1 mM $NO_3^-$ for 15 minutes. Ten minute after an exchange of the medium to a $NO_3^-$-free one, the FRET/CFP ratio had recovered to the initial level. Rate of FRET ratio changes in the cells were determined based on

the difference of the ratio at two point of time (Fig. 7B). Rates of changes were estimated to be 0.0011 – 0.0034 (average 0.0022; 18 cells) by addition 1 mM [$NO_3^-$] to DMEM medium, and 0.0011 – 0.0022 (average 0.0015; 18 cells) by removal of $NO_3^-$.

## DISCUSSION

*Biosensor employing a bacterial environmental response system*–NasS and NasT in the root nodule bacterium *B. japonicum* are involved in a two-component response system to environmental [$NO_3^-$] and regulate protein levels related to $NO_3^-$ assimilation (13). We exploited the change in their association-dissociation behavior depending on [$NO_3^-$] to develop a $NO_3^-$ biosensor. sNOOOpy is the first FRET-based biosensor derived from a bacterial environmental response system. Typically, bacterial two-component regulatory systems comprise a sensor histidine kinase and its cognate response regulator (25), and their functions are controlled by phosphorylation levels of the response regulator catalyzed by histidine kinase in response to environmental stimuli. On the other hand, the two-component system of NasS-NasT is regulated without phosphorylation, meaning the reaction is energetically reversible. The sNOOOpy system does not require any component, such as ATP or metal ions, for detection of the [$NO_3^-$] change, and can furthermore detect both an increase and decrease of [$NO_3^-$]. These results provide evidence that a potential biological function of the NasS-NasT two-component system is to respond to not only the increase but also the decrease of cellular [$NO_3^-$], allowing the bacteria to presumably suppress the protein transcription level.

An NasS-NasT-like two-component system, AmiC and AmiR, that regulates protein levels involved in the catabolic degradation of aliphatic amides was also found in *Pseudomonas aeruginosa* (26, 27). When considered with the development of the sNOOOpy system from NasS-NasT, we suggest the possibility of an aliphatic amide sensor derived from AmiC-AmiR.

*Sensitivity of the sNOOOpy system in vitro and in vivo*–$NO_3^-$/$NO_2^-$ are reported to be in micromolar levels in tissues, blood, and plasma (3 – 50 μM) (28), and in millimolar levels in urine (8). Therefore, to monitor the change in $NO_3^-$/$NO_2^-$ levels in physiological processes, indicators must have submicromolar to submillimolar sensitivity. When a protein concentration of 1 μM each of CFP-NasT and NasS-YFP is used, the sNOOOpy system can detect a change in [$NO_3^-$] in the micromolar range using our *in vitro* assay conditions. This detection limit of the sNOOOpy system is similar to that of the Griess method.

To determine whether the sNOOOpy system can work in mammalian cells, we subjected cells harboring sNOOOpy proteins to medium containing physiological concentrations of $NO_3^-$ or $NO_2^-$ (0.01 – 10 mM). Although little is known about influx and efflux of $NO_3^-$ from mammalian cells, the $NO_3^-$ influx and characteristics of sialin, a $2NO_3^-/H^+$ cotransporter, were investigated only in human submandibular gland cell line (HSG) cells (9). In the extracellular solution containing physiological concentrations of $NO_3^-$ (0.05 – 0.5 mM), a patch-clamp method detected an

anion current derived from $NO_3^-$ influx into HSG cells at low pH condition. Recently, the cell bank found that HSG are the originated from HeLa cells. Therefore, in this study, we exploited the HeLa cells for live cell $NO_3^-/NO_2^-$ imaging. While no obvious changes were observed up to 0.1 mM of $NO_3^-$, the FRET ratio of sNOOOpy was changed in response to 0.3 – 3 mM of $NO_3^-$ in the medium even at a neutral pH condition.

While >90% of CFP-NasT and NasS-YFP were dissociated in the presence of 1 mM of $NO_3^-$ *in vitro* assay conditions, the FRET ratios in the HeLa cells showed obvious changes at levels up to 3 mM in the medium. Furthermore, the rate of FRET/CFP ratio changes *in vitro* is 0.2 $s^{-1}$ by addition of 40 μM [$NO_3^-$] to assay condition, which was markedly faster than that in HeLa cells, 0.002 $s^{-1}$ by addition of 1 mM [$NO^{3-}$] to the medium. Here we consider some of the reasons for the differences of the sNOOOpy system between *in vitro* and *in vivo*. One possibility is that the cellular [$NO_3^-$] is not raised to the same level as that in the medium, so concentrations in the medium might not be accurately reflected in the HeLa cells. Another possibility is that the sensitivity of sNOOOpy is affected by some cellular environmental factors. Our results showed that excess of CFP-NasT protein increases $K_D$ values caused by an intermolecular FRET system. Such protein concentration dependency of sNOOOpy may be avoided by developing sNOOOpy to be an intramolecular system.

Among NasS-like proteins, crystallographic study of NrtA, $NO_3^-$ binding protein from cyanobacteria, has been reported (22), and residues involved in $NO_3^-$ binding were identified. In this study, we constructed sNOOOpy$^{H145A}$, which comprises NasS$^{H145A}$ mutant, and revealed an important role of the residue for $NO_3^-/NO_3^-$ responsiveness by sNOOOpy system. On the other hand, structural bases of the interaction of NasS with NasT are still unclear. Crystallographic studies are desired for further improvement in sensitivity and specificity of the sNOOOpy system.

Furthermore, strong base fluorescence emission might limit the detection sensitivity. Therefore, it might be possible to further improve FRET signal of sNOOOpy by using a polarized fluorescence excitation and detection technique (29).

*Insight for future applications of the sNOOOpy system*–As $NO_3^-$ and $NO_2^-$ are accepted as stable reservoirs that can be reduced to bioactive NO through the "$NO_3^-$-$NO_2^-$-NO pathway", the potential benefits of $NO_3^-/NO_2^-$ in the health field has received much attention. For example, recent prospective epidemiologic studies have shown that green leafy vegetables are protective against coronary heart disease and ischemic strokes (30, 31). Many researchers explained these effects using the biologically plausible hypothesis that $NO_3^-/NO_2^-$ in the diet can provide substrates for NO, which results in vasodilation, decreased blood pressure, and supported cardiovascular function (32–34). Thus, NO/$NO_3^-/NO_2^-$ studies have advanced rapidly in the last decade, and the possibility that these anions can be used as therapy for human diseases (*e.g.*, myocardial infarction, stroke, solid-organ transplantation, sickle-cell disease) has been suggested (3, 6, 35). Furthermore, Tang *et al.* suggested that determining endogenous $NO_3^-/NO_2^-$ levels is expected if

these anions can be used as diagnostic biomarkers of disease or treatment regimens (5). Unfortunately, despite the increased attention to the "$NO_3^-$-$NO_2^-$-NO pathway, no other methodology like that of the Griess reaction has been widely used.

We demonstrated that the sNOOOpy system is a $NO_3^-$/$NO_2^-$-specific biosensor that enables us to visualize both the increase and decrease in $NO_3^-$/$NO_2^-$ levels in mammalian cells (Fig. 7C). In particular, because the sNOOOpy system is applicable to living cells, which is unique compared to conventional measurement methods, sNOOOpy makes it possible to observe the intracellular dynamics of $NO_3^-$/$NO_2^-$ in both *in situ* and in real time. The sNOOOpy system paves the way for the elucidation of NO/$NO_3^-$/$NO_2^-$ biology. Finally, we refer to the potential usefulness of the sNOOOpy system for applications in bacteria and plants. $NO_3^-$/$NO_2^-$ serves as an essential nutrient for plant growth and survival, because of its involvement in several crucial biological functions of plants (*e.g.*, tissue development, immune systems). The visualization of $NO_3^-$/$NO_2^-$ dynamics in the physiological actions of plants by the sNOOOpy system has the potential to contribute to the elucidation of fundamental and applied mechanisms of plant life.

**Acknowledgments:** We wish to thank Cristina Sánchez and Manabu Itakura for their help with the preparation of this technology, Takeharu Nagai for plasmids of CFP and YFP.

**Conflict of interest:** The authors declare that they have no conflicts of interest with the contents of this article.

**Author Contributions:** A.G., M.H., T.S., H.I. performed the experiments. A.G., M.H. and H.I. analyzed the results. K.M. provided the materials. A.G., M.H. and T.U. were involved in the design of the study. A.G., M.H., H.I., and T.U. wrote the paper.

## References

1. Ignarro, L. J., Fukuto, J. M., Griscavage, J. M., Rogers, N. E., and Byrns, R. E. (1993) Oxidation of nitric oxide in aqueous solution to nitrite but not nitrate: comparison with enzymatically formed nitric oxide from L-arginine. *Proc. Natl. Acad. Sci. U. S. A.* **90**, 8103–8107

2. Nathan, C. (1992) Nitric oxide as a secretory product of mammalian cells. *FASEB J.* **6**, 3051–3064

3. Lundberg, J. O., Weitzberg, E., and Gladwin, M. T. (2008) The nitrate – nitrite – nitric oxide pathway in physiology and therapeutics. *Crit. Care Med.* **7**, 156–167

4. Shiav, S. (2013) Nitrite: A physiological store of nitric oxide and modulator of mitochondrial function. *Redox Biol.* **1**, 40–44

5. Tang, Y., Jiang, H., and Bryan, N. S. (2011) Nitrite and nitrate: cardiovascular risk-benefit and metabolic effect. *Curr. Opin. Lipidol.* **22**, 11–15

6. Lundberg, J. O., Gladwin, M. T., Ahluwalia, A., Benjamin, N., Bryan, N. S., Butler, A., Cabrales, P., Fago, A., Feelisch, M., Ford, P. C., Freeman, B. a, Frenneaux, M., Friedman, J., Kelm, M., Kevil, C. G., Kim-Shapiro, D. B., Kozlov, A. V, Lancaster, J. R., Lefer, D. J., McColl, K., McCurry, K., Patel, R. P., Petersson, J., Rassaf, T., Reutov, V. P., Richter-Addo, G. B., Schechter, A., Shiva, S., Tsuchiya, K., van Faassen, E. E., Webb, A. J., Zuckerbraun, B. S., Zweier, J. L., and Weitzberg, E. (2009) Nitrate and nitrite in biology, nutrition and therapeutics. *Nat. Chem. Biol.* **5**, 865–869

7. Giustarini, D., Rossi, R., Milzani, A., and Dalle-Donne, I. (2008) Nitrite and Nitrate Measurement by Griess Reagent in Human Plasma: Evaluation of Interferences and Standardization. *Methods Enzymol.* **440**, 361–380

8. Tsikas, D. (2007) Analysis of nitrite and nitrate in biological fluids by assays based on the Griess reaction: Appraisal of the Griess reaction in the l-arginine/nitric oxide area of research. *J. Chromatogr. B Anal. Technol. Biomed. Life Sci.* **851**, 51–70

9. Qin, L., Liu, X., Sun, Q., Fan, Z., Xia, D., Ding, G., Ong, H. L., Adams, D., Gahl, W. a., Zheng, C., Qi, S., Jin, L., Zhang, C., Gu, L., He, J., Deng, D., Ambudkar, I. S., and Wang, S. (2012) From the Cover: Sialin (SLC17A5) functions as a nitrate transporter in the plasma membrane. *Proc. Natl. Acad. Sci.* **109**, 13434–13439

10. Romeo, a., Sonnleitner, E., Sorger-Domenigg, T., Nakano, M., Eisenhaber, B., and Blasi, U. (2012) Transcriptional regulation of nitrate assimilation in Pseudomonas aeruginosa occurs via transcriptional antitermination within the nirBD-PA1779-cobA operon. *Microbiology*. **158**, 1543–1552

11. Luque-Almagro, V. M., Lyall, V. J., Ferguson, S. J., Roldán, M. D., Richardson, D. J., and Gates, A. J. (2013) Nitrogen oxyanion-dependent dissociation of a two-component complex that regulates bacterial nitrate assimilation. *J. Biol. Chem.* **288**, 29692–29702

12. Wang, B., Pierson, L. S., Rensing, C., Gunatilaka, M. K., and Kennedy, C. (2012) NasT-mediated antitermination plays an essential role in the regulation of the assimilatory nitrate reductase operon in azotobacter vinelandii. *Appl. Environ. Microbiol.* **78**, 6558–6567

13. Sánchez, C., Itakura, M., Okubo, T., Matsumoto, T., Yoshikawa, H., Gotoh, A., Hidaka, M., Uchida, T., and Minamisawa, K. (2014) The nitrate-sensing NasST system regulates nitrous oxide reductase and periplasmic nitrate reductase in Bradyrhizobium japonicum. *Environ. Microbiol.* **16**, 3263–3274

14. Kaneko, T., Nakamura, Y., Sato, S., Minamisawa, K., Uchiumi, T., Sasamoto, S., Watanabe, A., Idesawa, K., Iriguchi, M., Kawashima, K., Kohara, M., Matsumoto, M., Shimpo, S., Tsuruoka, H., Wada, T., Yamada, M., and Tabata, S. (2002) Complete genomic sequence of nitrogen-fixing symbiotic bacterium Bradyrhizobium japonicum USDA110. *DNA Res.* **9**, 189–197

15. Nagai, T., Yamada, S., Tominaga, T., Ichikawa, M., and Miyawaki, A. (2004) Expanded dynamic range of fluorescent indicators for Ca(2+) by circularly permuted yellow fluorescent proteins. *Proc. Natl. Acad. Sci. U. S. A.* **101**, 10554–10559

16. Cubitt, A. B., Woollenweber, L. A., and Heim, R. (1999) Understanding structure-function relationships in the Aequorea victoria green fluorescent protein. *Methods Cell Biol.* **58**, 19–30

17. Patterson, G., Day, R. N., and Piston, D. (2001) Fluorescent protein spectra. *J. Cell Sci.* **114**, 837–838

18. Martin, S. F., Tatham, M. H., Hay, R. T., and Samuel, I. D. W. (2008) Quantitative analysis of multi-protein interactions using FRET: application to the SUMO pathway. *Protein Sci.* **17**, 777–784

19. Matsuda, T., Miyawaki, A., and Nagai, T. (2008) Direct measurement of protein dynamics inside cells using a rationally designed photoconvertible protein. *Nat. Methods*. **5**, 339–345

20. Nagai, T., Ibata, K., Park, E. S., Kubota, M., Mikoshiba, K., and Miyawaki, A. (2002) A variant of yellow fluorescent protein with fast and efficient maturation for cell-biological applications. *Nat. Biotechnol.* **20**, 87–90

21. Zacharias, D. A., Violin, J. D., Newton, A. C., and Tsien, R. Y. (2002) Partitioning of lipid-modified monomeric GFPs into membrane microdomains of live cells. *Science*. **296**, 913–916

22. Koropatkin, N. M., Pakrasi, H. B., and Smith, T. J. (2006) Atomic structure of a nitrate-binding protein crucial for photosynthetic productivity. *Proc. Natl. Acad. Sci. U. S. A.* **103**, 9820–9825

23. Kim, J. H., Lee, S. R., Li, L. H., Park, H. J., Park, J. H., Lee, K. Y., Kim, M. K., Shin, B. A., and Choi, S. Y. (2011) High cleavage efficiency of a 2A peptide derived from porcine teschovirus-1 in human cell lines, zebrafish and mice. *PLoS One*. **6**, 1–8

24. Szymczak, A. L., Workman, C. J., Wang, Y., Vignali, K. M., Dilioglou, S., Vanin, E. F., and Vignali, D. a a (2004) Correction of multi-gene deficiency in vivo using a single "self-cleaving" 2A peptide-based retroviral vector. *Nat. Biotechnol.* **22**, 589–594

25. West, A. H., and Stock, A. M. (2001) Histidine kinases and response regulator proteins in two-component signaling systems. *Trends Biochem. Sci.* **26**, 369–376

26. O'Hara, B. P., Norman, R. a., Wan, P. T. C., Roe, S. M., Barrett, T. E., Drew, R. E., and Pearl, L. H. (1999) Crystal structure and induction mechanism of AmiC-AmiR: A ligand-regulated transcription antitermination complex. *EMBO J.* **18**, 5175–5186

27. Wilson, S. a, Wachira, S. J., Norman, R. a, Pearl, L. H., and Drew, R. E. (1996) Transcription antitermination regulation of the Pseudomonas aeruginosa amidase operon. *EMBO J.* **15**, 5907–5916

28. Bryan, N. S., Rassaf, T., Maloney, R. E., Rodriguez, C. M., Saijo, F., Rodriguez, J. R., and Feelisch, M. (2004) Cellular targets and mechanisms of nitros(yl)ation: an insight into their nature and kinetics in vivo. *Proc. Natl. Acad. Sci. U. S. A.* **101**, 4308–4313

29. Rizzo, M. a, and Piston, D. W. (2005) High-contrast imaging of fluorescent protein FRET by fluorescence polarization microscopy. *Biophys. J.* **88**, L14–L16

30. Joshipura, K. J., Hu, F. B., Manson, J. E., Stampfer, M. J., Rimm, E. B., Speizer, F. E., Colditz, G., Ascherio, A., Rosner, B., Spiegelman, D., and Willett, W. C. (2001) The effect of fruit and vegetable intake on risk for coronary heart disease. *Ann.Intern.Med.* **134**, 1106–1114

31. Joshipura, K. J., Ascherio, A., Manson, J. E., Stampfer, M. J., Rimm, E. B., Speizer, F. E., Hennekens, C. H., Spiegelman, D., and Willett, W. C. (1999) Fruit and vegetable intake in relation to risk of ischemic stroke. *JAMA*. **282**, 1233–1239

32. Hord, N. G., Tang, Y., and Bryan, N. S. (2009) Food sources of nitrates and nitrites: the physiologic contact for potential health benefits. *Am J Clin Nutr*. **90**, 1–10

33. Lundberg, J. O., Feelisch, M., Björne, H., Jansson, E. Å., and Weitzberg, E. (2006) Cardioprotective effects of vegetables: Is nitrate the answer? *Nitric Oxide - Biol. Chem.* **15**, 359–362

34. McKnight, G. M., Duncan, C. W., Leifert, C., and Golden, M. H. (1999) Dietary nitrate in man: friend or foe? *Br. J. Nutr.* **81**, 349–358

35. Butler, A. R., and Feelisch, M. (2008) Therapeutic uses of inorganic nitrite and nitrate: From the past to the future. *Circulation.* **117**, 2151–2159

36. Sievers, F., Wilm, A., Dineen, D., Gibson, T. J., Karplus, K., Li, W., Lopez, R., McWilliam, H., Remmert, M., Soding, J., Thompson, J. D., and Higgins, D. G. (2014) Fast, scalable generation of high-quality protein multiple sequence alignments using Clustal Omega. *Mol. Syst. Biol.* **7**, 539–539

37. Robert, X., and Gouet, P. (2014) Deciphering key features in protein structures with the new ENDscript server. *Nucleic Acids Res.* **42**, W320–W324



## FOOTNOTES

T.U. was supported by the Grant-in-Aid for Scientific Research (A) (26252064), Grant-in-Aid for Challenging Exploratory Research (26660287) from the Ministry of Education, Culture, Sports, Science, and Technology of Japan, and Science and Technology Research Promotion Program for Agriculture, Forestry, Fisheries, and Food Industry (25028A). M.H. was supported by the Grant-in-Aid for Young Scientist (B) (24780092, 26850042) from the Ministry of Education, Culture, Sports, Science, and Technology of Japan, and K.M. was supported by BRAIN and the Grant-in-Aid for Scientific Research (A) (26252065) from the Ministry of Education, Culture, Sports, Science, and Technology of Japan.

The abbreviations used are: CFP, cyan fluorescent protein; FRET, fluorescence resonance energy transfer; sNOOOpy, sensor for $NO_3^-$/$NO_2^-$ in physiology; YFP, yellow fluorescent protein.

## FIGURE LEGENDS

**Figure 1.** FRET-based $NO_3^-$/$NO_2^-$ probes, sNOOOpy. (A) Proposed model of a two-component regulatory system composed of NasS-NasT. NasS plays a negative regulatory role by interacting with NasT. In the presence of $NO_3^-$ or $NO_2^-$, the putative RNA-binding protein NasT is released from NasS and acts as a transcription antiterminator that binds the leader sequence in mRNA, preventing hairpin formation and allowing complete transcription of the genes. (B) Schematic drawing of the sNOOOpy

system. CFP and YFP (Venus) are connected with NasT and NasS, respectively. In the $NO_3^-$/$NO_2^-$-free form (left), the formation of a stable dimer between NasT-NasS draws the two fluorescent proteins close to each other, resulting in high FRET efficiency. In the $NO_3^-$ or $NO_2^-$-bound form, dissociation of the two proteins separates the two fluorescent proteins, which decreases FRET efficiency. F. I., fluorescence intensity. (C) Schematic diagram of sNOOOpy proteins, CFP-NasT and NasS-YFP (Venus_cp195). (D) FRET/CFP ratio changes in NasS fused with different Venus variants. Fluorescent emissions of NasS fused with Venus variants (1 μM) were measured in the presence of CFP (1 μM) (open square), CFP-NasT (1 μM) (closed square), or CFP-NasT with 2 μM of $NO_3^-$ (gray square). The labels 50, 157, 173, 195, and 229 indicate circularly permuted Venus having the 50$^{th}$, 157$^{th}$, 173$^{rd}$, 195$^{th}$ and 229$^{th}$ amino acid as its N-terminus, respectively. (E, F) Fluorescence emissions of sNOOOpy. Fluorescence were measured by excitation with 410 nm (left and middle) or 475 nm (right) light at various concentrations of (E) $NO_3^-$ and (F) $NO_2^-$ at 25 °C using protein pairs of 1 μM each of CFP-NasT + NasS-YFP (left), or CFP-NasT + His-tagged NasS (middle), or GST-tagged NasT + NasS-YFP (middle and right) in 100 mM HEPES-NaOH pH 8.0 and 10 mM KCl. Emissions of sNOOOpy-ΔNasT, which is composed of CFP and NasT-YFP, are shown as broken lines.

**Figure 2.** Specificities of the sNOOOpy system. FRET/CFP ratio of sNOOOpy in the presence of 0 (gray), 100 μM (green), 10 mM (red), and 100 μM $NO_3^-$ with 10 mM of each anion (yellow) is shown. Solid and broken line indicates FRET/CFP ratio of sNOOOpy with 100 μM $NO_3^-$ and sNOOOpy-ΔNasT, which is composed of CFP and NasT-YFP, respectively.

**Figure 3.** Characterizations of NasS-NasT interaction by sNOOOpy system *in vitro*. (A) Fluorescence emissions at 535 nm from the NasS-NasT binding assay using multi-well plates on a TECAN Spark 10M (excitation filter: 405 ± 10 nm, emission filter: 535 ± 10 nm). Emission of 1 μM CFP-NasT in the absence of NasS-YFP is shown as solid line and labeled (1). Emissions of various [NasS-YFP] in the absence (cyan, labeled (2)) or presence of 1 μM CFP-NasT (red, labeled (3)) were plotted. Sums of emissions (1) and (2) were shown in blue. (B) Emissions derived from FRET. FRET emissions were estimated from plots of (A) by FRET emission = (3) − {(1) + (2)} in (A) as in *Ref.* (18). The plots were fitted with a single binding model,

$$E = E_{\max} \times \frac{\left[K_{\mathrm{ST}} + [\mathrm{S}]_{\mathrm{total}} + [\mathrm{T}]_{\mathrm{total}} - \sqrt{(K_{\mathrm{ST}} + [\mathrm{S}]_{\mathrm{total}} + [\mathrm{T}]_{\mathrm{total}})^2 - 4 \times [\mathrm{S}]_{\mathrm{total}} \times [\mathrm{T}]_{\mathrm{total}}}\right]}{2}$$

where $E$ is the fluorescent emission at 535 nm, $K_{\mathrm{ST}}$ is dissociation constant between CFP-NasT and NasS-YFP, $[\mathrm{S}]_{\mathrm{total}}$ is the total NasS-YFP, and $[\mathrm{T}]_{\mathrm{total}}$ is the total CFP-NasT (= 1 μM) concentrations, respectively. $K_{\mathrm{ST}}$ was calculated by the fit. (C) Titration analyses of sNOOOpy (1 μM each of CFP-NasT + NasS-YFP) with unlabeled NasS. (D) Competitive reaction model of sNOOOpy adopted for this study. NasS-YFP is involved in two binding equilibria at steady-state: complex formation with CFP-NasT (*Eq.* 1), or $NO_3^-$ or $NO_2^-$ (*Eq.* 2). The constants $K_{\mathrm{ST}}$ and $K_{\mathrm{S\text{-}NO3}}$ are dissociation constants

from *Eq*. 1 and *Eq*. 2, respectively. (E) Fluorescence emissions of various [CFP-NasT] in the absence (cyan) or presence of 1 μM NasS-YFP at various [$NO_3^-$]. Emissions at 535 nm were measured using multi-well plates as in (A). (F) Emissions derived from FRET were estimated from plots of (E) as in (B). (G) Relative FRET emissions at various [$NO_3^-$] relative to those in the absence of [$NO_3^-$] were plotted against [CFP-NasT].

**Figure 4.** Sensitivities of sNOOOpy *in vitro*. (A) $NO_3^-$ binding site structure of NrtA. Bound $NO_3^-$ is shown as a sphere model. Side chain of the H196 that form direct interaction with $NO_3^-$ is shown. The residue name and numbers in parentheses indicate the corresponding residue in NasS. This image was prepared using PyMOL (DeLano Scientific, Palo Alto, CA). Amino acid sequence alignment between NasS and NrtA are shown in the bottom panel. The residues involved in binding of a nitrate are indicated by blue dots. The sequences were aligned with CLUSTAL OMEGA (36), and this image was prepared using ESPript (37). (B) FRET/CFP ratio of sNOOOpy$^{WT}$ (WT) and sNOOOpy$^{H145A}$ (H145A) plotted against increasing concentrations of $NO_3^-$ (red) and $NO_2^-$ (blue). Values in parentheses indicate the $K_D$ values for $NO_3^-$ (red) and $NO_2^-$ (blue), the values at which the [$NO_3^-$] or [$NO_2^-$] dissociates half of the NasST. Concentrations of 1 μM of sNOOOpy protein, composed of equal concentrations of CFP-NasT and NasS-YFP, were used. The $K_D$ values are calculated by curve-fitting analysis using the standard Hill equation. (C) FRET/CFP ratios at various concentrations of [CFP-NasT] were plotted against increasing [$NO_3^-$]. Concentrations of 1 μM of NasS-YFP and 0.5 – 2.0 μM of CFP-NasT were used. (D) $K_D$ values were plotted against [CFP-NasT] and fitted by equation: $K_D = (1 + [\text{CFP-NasT}]/K_{ST}) \times K_{S\text{-}NO3}$. From linear fit to the plot, $K_{S\text{-}NO3}$, $K_{ST}$, and $K_{S\text{-}NO3}/K_{ST}$, were calculated as 6.0 μM, 0.15 μM, and 39, respectively.

**Figure 5.** Characterizations of sNOOOpy. (A) Time course of the FRET/CFP ratio change in the presence of various concentrations of $NO_3^-$. (B) Apparent rate constant ($k^{app} = k_{on}[NO_3^-] + k_{off}$) were plotted against [$NO_3^-$]. From linear fit to the plot, $k_{on}$ and $k_{off}$ were calculated as 0.0023 $\mu M^{-1}s^{-1}$ and 0.10 $s^{-1}$, respectively. (C) pH and (D) temperature dependencies of sNOOOpy. The values of $R_0$ and $R_{\Delta NasT}$ indicate the emission ratio of control (in the anion-free buffer) and that of sNOOOpy-ΔNasT, respectively. The FRET/CFP ratio at 25 °C at 0, 10, 100, and 1000 μM $NO_3^-$ in the pH range of 6.0 – 9.0 are shown. The buffer contained 100 mM MES-NaOH (pH 6.0 – 7.0, open circles) or HEPES-NaOH (pH 7.0 – 9.0, closed circle). (E) Kinetic analyses of sNOOOpy$^{WT}$ *in vitro* at 25 °C (black) and 37 °C (red). FRET/CFP ratio of plotted against increasing concentrations of $NO_3^-$. Concentrations of 1 μM of sNOOOpy protein, which was composed of equal concentrations of CFP-NasT and NasS-YFP, were used.

**Figure 6.** Monitoring the cytoplasmic $NO_3^-$ levels of HeLa cells. (A) Schematic diagram of pCMV-sNOOOpy, the plasmid for mammalian expression, contains a nuclear export signal fused to

CFP-NasT and NasS-YFP, and they linked by a self-processing 2A peptide. (B) Expression of the sNOOOpy system proteins in HeLa cells. CFP-NasT and NasS-YFP were detected by Western blot analysis of the lysates from HeLa cells harboring pCMV-sNOOOpy$^{WT}$. pCMV-sNOOOpy was transfected into the HeLa cells with the Lipofectamine 2000 transfection reagent. Western blot analysis was performed 48 h after transfection. CFP-NasT (estimated molecular weight 69.3 kDa) and NasS-YFP (50.2 kDa) were detected after probing with a GFP(FL) rabbit polyclonal IgG (Santa Cruz Biotechnology, Inc.) followed by an anti-rabbit IgG HRP-linked antibody (Cell Signaling Technology). (C) Sequential images of the FRET/CFP emission ratio (pseudocolored) of HeLa cells expressing sNOOOpy$^{WT}$ (top and middle) and sNOOOpy$^{H145A}$ (bottom). Total elapsed time (in min) is shown at the top left of the cells. Concentrations of 0.3 mM, 1 mM, and 3 mM $NO_3^-$ (top and bottom) and $NO_2^-$ (middle) were added to the medium at time = 10, 20, 30 (min), respectively. (D) Time course of the FRET/CFP ratio changes in single cell expressing sNOOOpy$^{WT}$ over a wide range of $NO_3^-$ concentrations (0 – 10 mM). Concentrations of 0.01 mM, 0.1 mM, 1 mM, and 10 mM $NO_3^-$ were added to the medium at time = 15, 30, 45, 60 (min), respectively. FRET/CFP ratios in each cell and averaged ratio are shown in left and right panel, respectively. Error bars are standard deviations between measurements. (E) Time course of the FRET/CFP ratio changes in single cell. Concentrations of $NO_3^-$ in DMEM medium were changed as in (C). Ratios in each cell with sNOOOpy$^{WT}$ in (1) $NO_3^-$, in (2) $NO_2^-$, and (3) sNOOOpy$^{H145A}$ in $NO_3^-$ are shown. Averaged ratios are shown in right panel.

**Figure 7.** Detecting the dynamics of cellular $NO_3^-$ level. (A) Sequential images of the FRET/CFP emission ratio (pseudocolored) of HeLa cells expressing sNOOOpy$^{WT}$ are shown. At time = 0 (min), 1 mM $NO_3^-$ was added to the medium. After 15 min, the medium was exchanged for $NO_3^-$-free medium. (B) Time course of the FRET/CFP ratio in single cell. Concentrations of $NO_3^-$ in DMEM medium were changed as in (A). Ratios in each cell and averaged ratio were shown in left and right panel, respectively. Error bars are standard deviations between measurements. (C) Graphic representation of sNOOOpy system in living cells. This system enables to detect both increase and decrease of $NO_3^-$ level in mammalian cell as a FRET signal change.

**Table 1. Oligonucleotide primers used in this study.**

| Amplified gene/vector | Forward | Reverse |
|---|---|---|
| *pCold_CFP, pCold_CFP-NasT* | | |
| pCold-vector | 5'-**tag gta atc tct gct taa aag**-3' | 5'-**cat atg cct acc ttc gat atg**-3' |
| seCFP (pCold_CFP) | 5'-**cga agg tag gca tat g**gt gag caa ggg cg-3' | 5'-**gca gag att acc ta**t ctg tac agc tcg tcc atg c-3' |
| seCFP (pCold_CFP-NasT) | 5'-**cga agg tag gca tat g**gt gag caa ggg cg-3' | 5'-**cag gta cag ctc gtc cat gcc**-3' |
| NasT | 5'-**cat gga cga gct gta cat g**ag cgc cga gca g-3' | 5'-**ctt tta agc aga gat tac cta** ttt cag cat ctc cga c-3' |
| *pCold_NasS-Venus* | | |
| pCold-vector | 5'-**cac cac cac cac cac cac tag gta atc**-3' | 5'-**ggt gta tta cct c** |
| NasS | 5'-**gag gta ata cac c**at gac cgg acc gct tc -3' | 5'-**ggc ctt cca gcg acc**-3' |
| Venus | 5'-**ggt cgc tgg aag gcc** atg gtg agc aag ggc-3' | 5'-**gat tac cta gtg gtg gtg gtg gtg gtg** gcc acc gct gcc acc-3' |
| Venus_cp50 | 5'-**ggt cgc tgg aag gcc** acc ggc aag ctg ccc-3' | 5'-**gat tac cta gtg gtg gtg gtg gtg gtg** ggt gca gat cag ctt c-3' |
| Venus_cp157 | 5'-**ggt cgc tgg aag gcc** cag aag aac ggc atc-3' | 5'-**gat tac cta gtg gtg gtg gtg gtg gtg** ctt gtc ggc ggt gat ata g-3' |
| Venus_cp173 | 5'-**ggt cgc tgg aag gcc** atg gac ggc ggc gtg-3' | 5'-**ctt tta agc aga gat tac cta gtg gtg gtg gtg gtg gtg** ctc gat gtt gtg gcg-3' |
| Venus_cp195 | 5'-**ggt cgc tgg aag gcc** ctg ccc gac aac cac-3' | 5'-**gat tac cta gtg gtg gtg gtg gtg gtg** cag cac ggg gcc gtc-3' |
| Venus_cp229 | 5'-**ggt cgc tgg aag gcc** atc act ctc ggc atg-3' | 5'-**gat tac cta gtg gtg gtg gtg gtg gtg** ccc ggc ggc ggt cac-3' |
| *Mutant* | | |
| NasS(H145A) | 5'-ctt tcc gtt ctc gac cgc caa tta cca att gcg g-3' | 5'-ccg caa ttg gta att ggc ggt cga gaa cgg aaa g-3' |
| *pCMV_2Apeptide and pCMV_sNOOOpy*[1)] | | |
| pFLAG-CMV1[2)] | 5'-cag gct gga gac gtg gag gag aac | 5'-ctt cag cag gct gaa gtt agt agc tcc |

| | | |
|---|---|---|
| | cct gga cct gca tcc ctg tga ccc ctc ccc agt gcc tct c-3’ | gct tcc ggt aga tca att ctg acg gtt cac taa acg-3’ |
| pCMV_2Apeptide | 5’-**gtc gga gat gct gaa a**gg aag cgg agc tac taa c-3’ | 5’-**ggt aga tca att ctg**-3’ |
| CFP-NasT[3)] | 5’-**cag aat tga tct acc** atg ctg ccc ccc ctg gaa aga ctg acc ctg agc agc ggc atg gtg agc aag ggc-3’ | 5’-**ttt cag cat ctc cga c**-3’ |
| pCMV_CFP-NasT | 5’-**gca tcc ctg tga ccc**-3’ | 5’-**gaa gcg gtc cgg tca t**ag gtc cag ggt tct c-3’ |
| NasS-Venus_cp195 | 5’-**atg acc gga ccg ctt c**-3’ | 5’-**ggg tca cag gga tgc** cag cac ggg gcc gtc-3’ |

The letters in bold represent the overlap sequence in the In-Fusion reaction.

1) To construct pCMV_sNOOOpy, a pCMV_2A peptide was primarily constructed. Then, the genes in the order of *CFP-NasT* and *NasS-Venus(cp195)* were cloned into the pCMV_2A peptide.

2) The underlined letters represent the sequence coding the 2A peptide.

3) The underlined letters represent the sequence coding the nuclear export signal sequence.

**Table 2. sNOOOpy variants constructed in this study.**

| name | Component proteins | Characteristics *in vitro* |
|---|---|---|
| sNOOOpy-ΔNasT | CFP,<br>NasS-Venus_cp195 | Negative control. |
| sNOOOpy$^{WT}$ | CFP-NasT,<br>NasS-Venus_cp195 | Wild-type sNOOOpy that subjected to characterizations. |
| sNOOOpy$^{H145A}$ | CFP-NasT,<br>NasS(H145A)-Venus_cp195 | Form stable dimer that is not dissociated by $NO_3^-$/$NO_2^-$. |

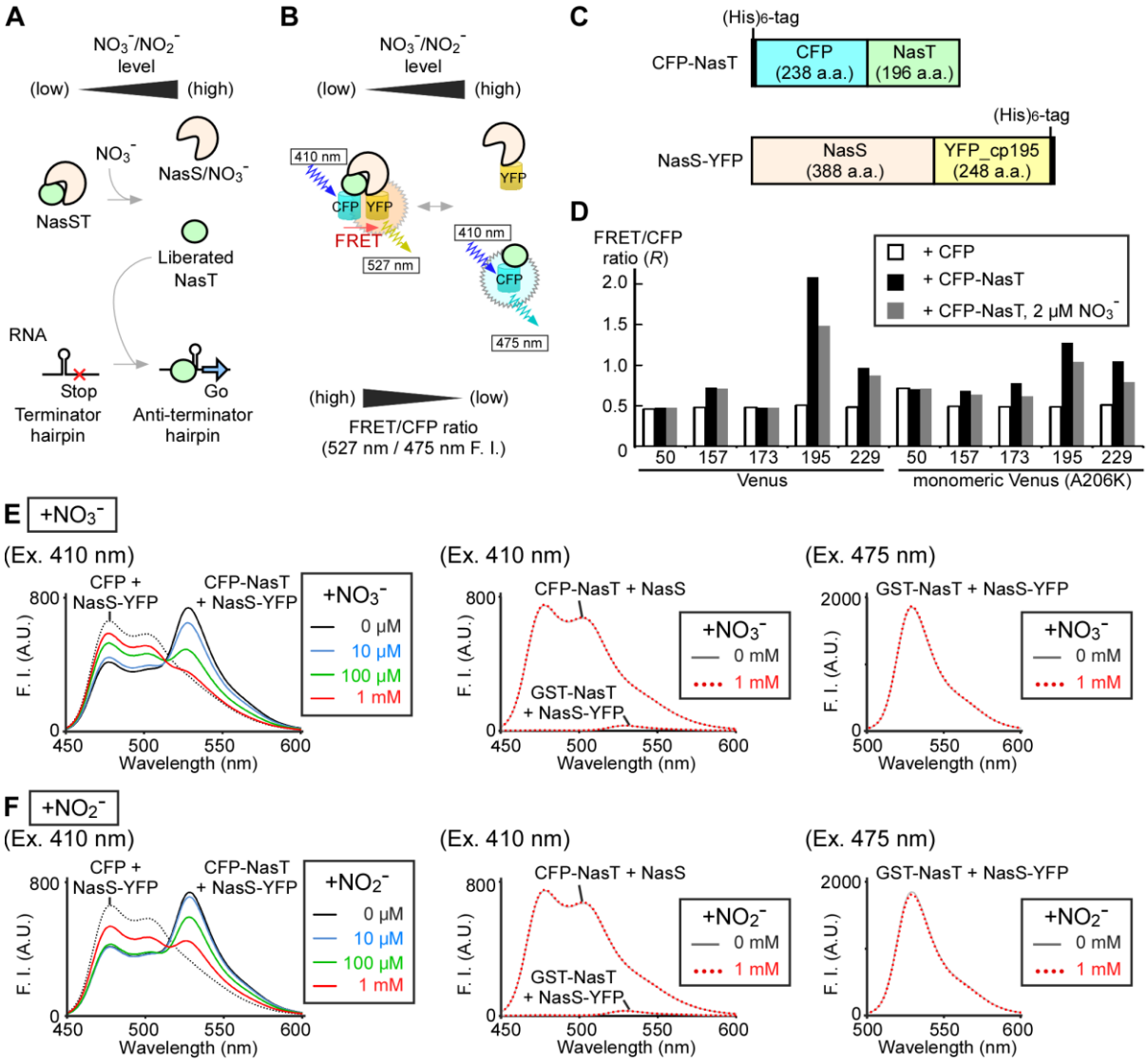


Figure 1

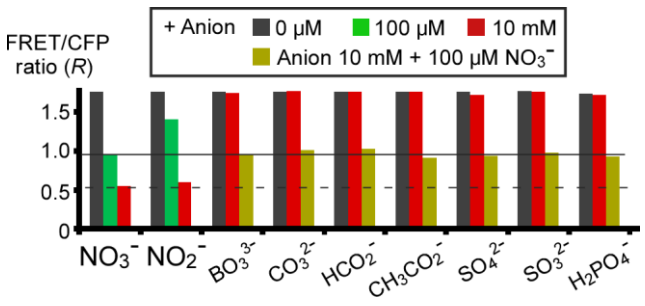


Figure 2

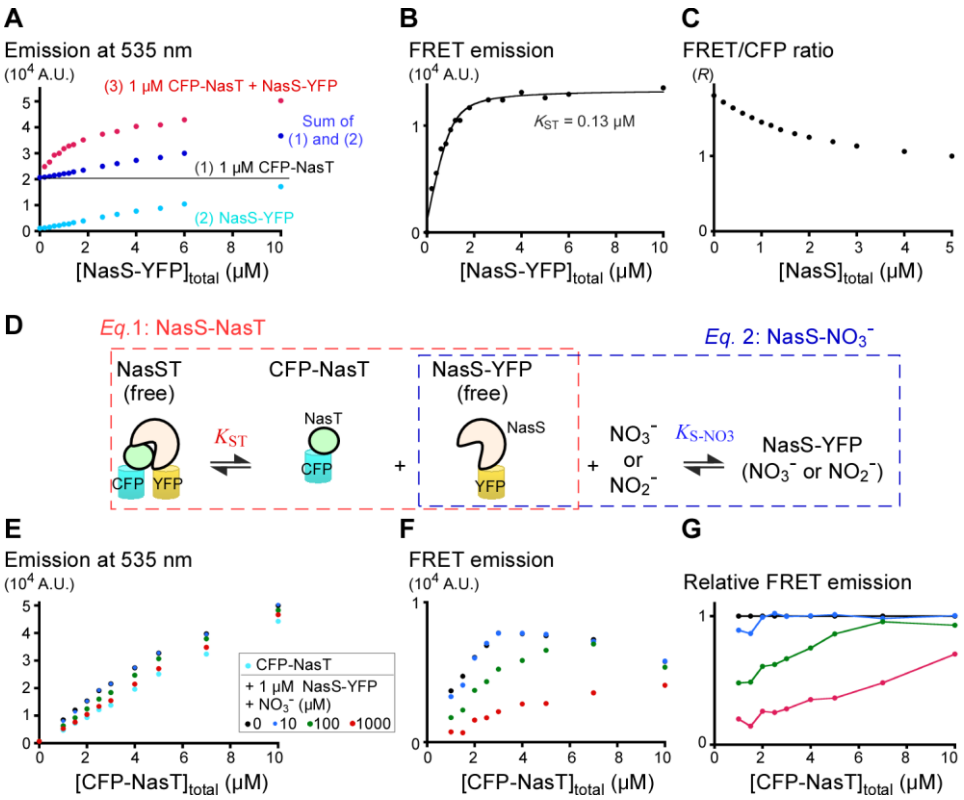


Figure 3.

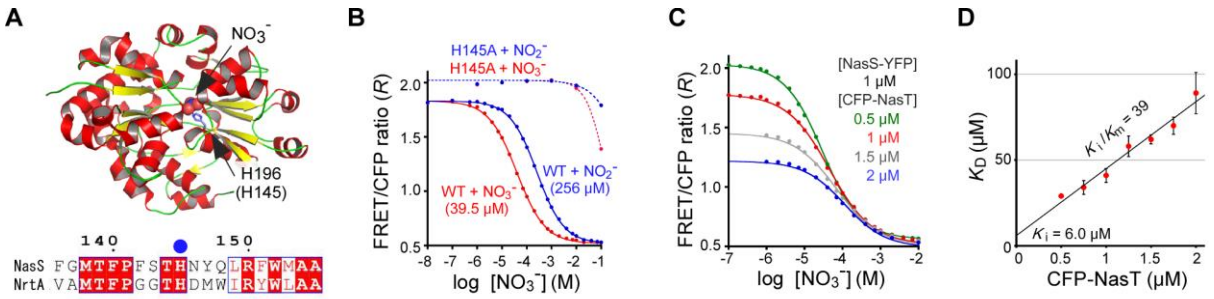


Figure 4.

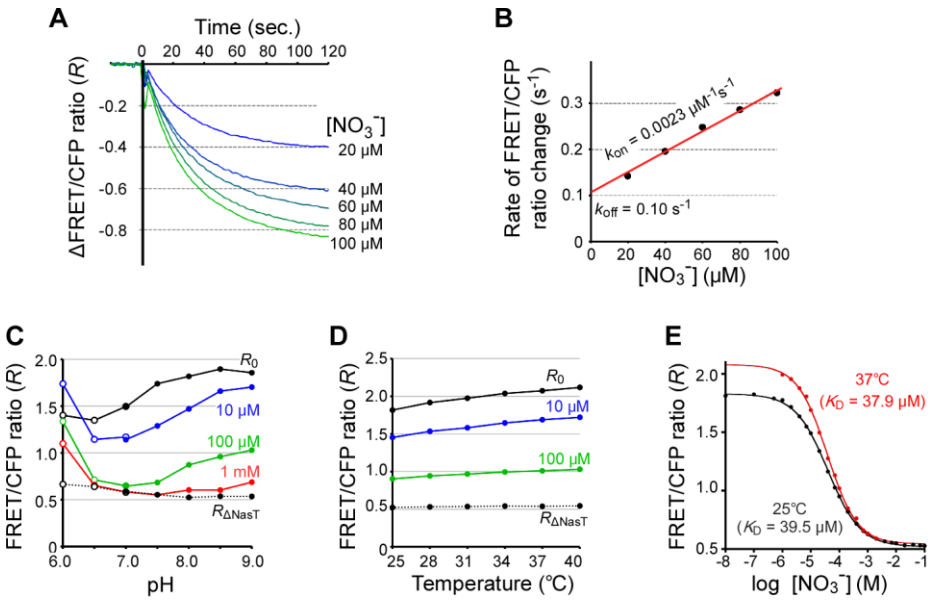


Figure 5.

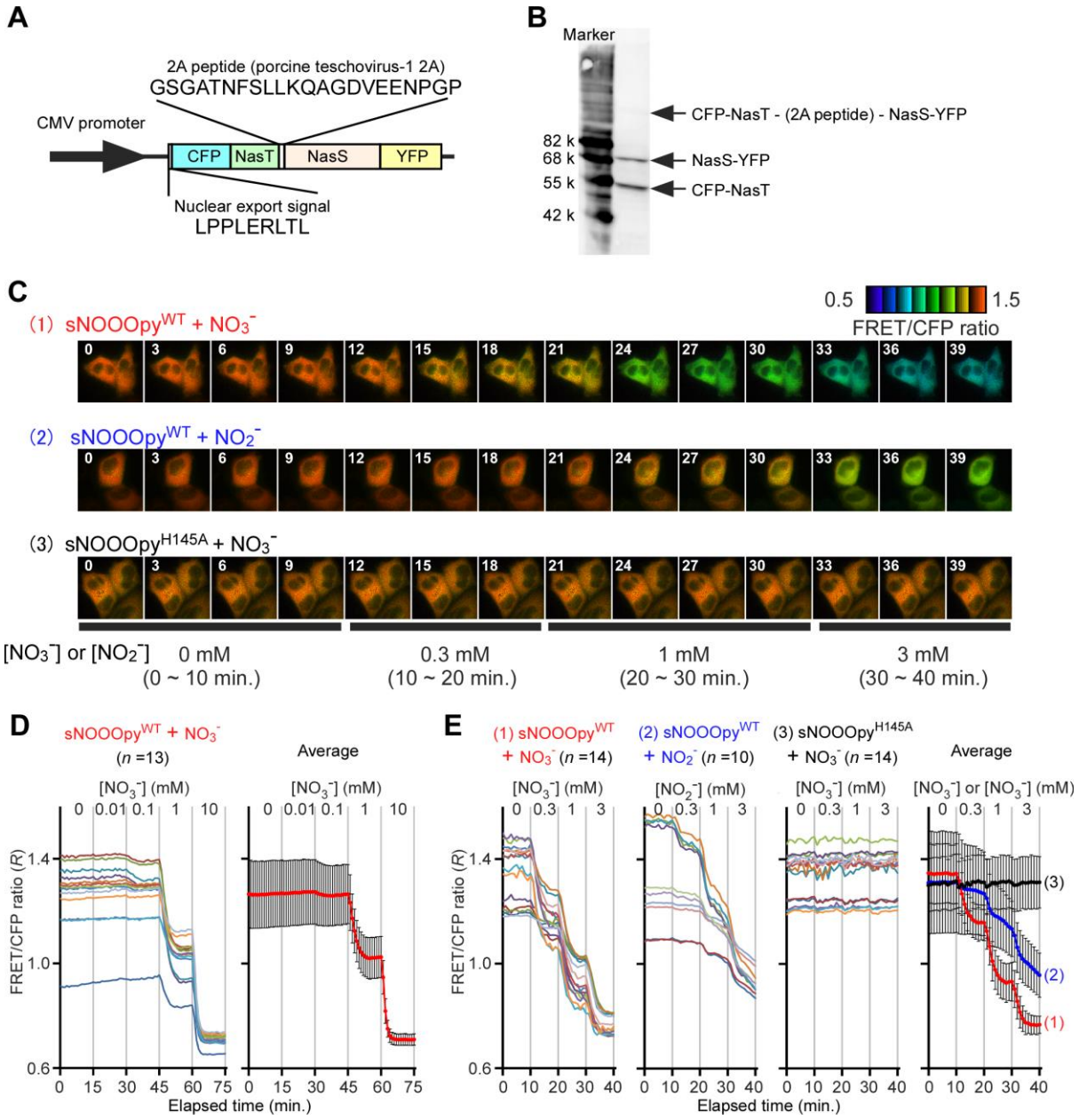


Figure 6.

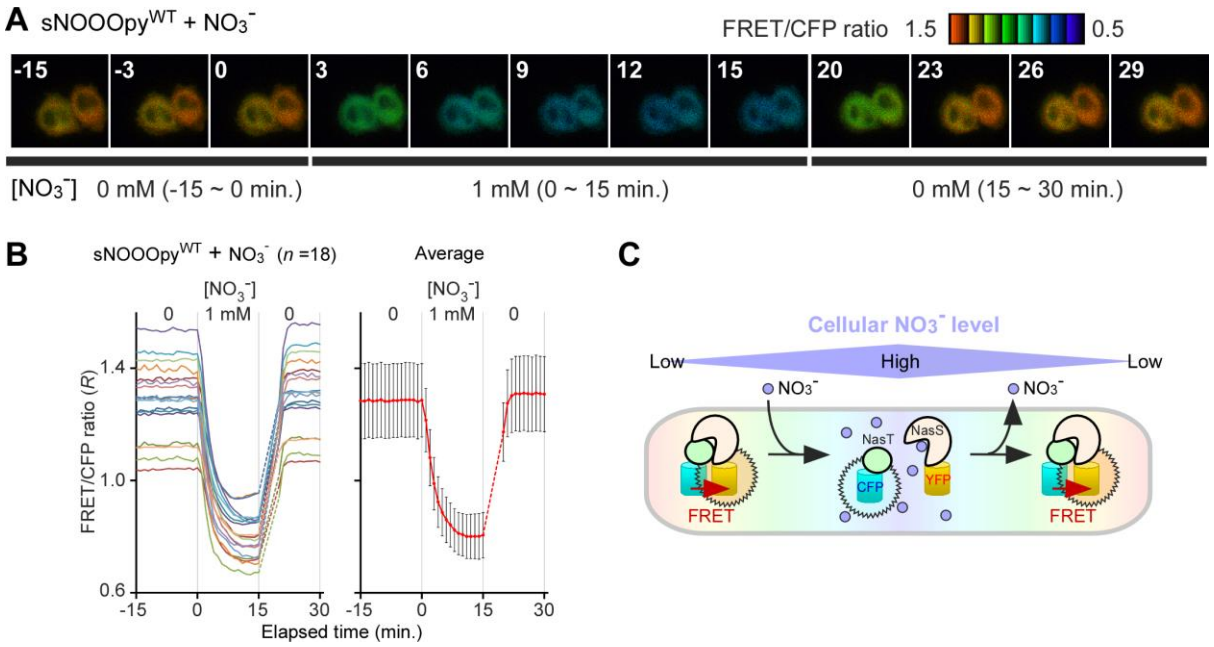


Figure 7.

**Supplementary Movie 1**

The FRET/CFP emission ratio (pseudocolored) of HeLa cells expressing sNOOOpy$^{WT}$. Total elapsed time (in min) is shown at the top left of the cells. Concentrations of 0.3 mM, 1 mM, and 3 mM $NO_3^-$ were added to the medium at time = 10, 20, 30 (min), respectively.

**Supplementary Movie 2**

Detection of the change in [$NO_3^-$] in DMEM medium by the sNOOOpy system.The FRET/CFP emission ratio (pseudocolored) of HeLa cells expressing sNOOOpy$^{WT}$ are shown. At time = 0 (min), 1 mM $NO_3^-$ was added to the medium. After 15 min, the medium was exchanged for $NO_3^-$-free medium.

Protein Structure and Folding:

# Visualization of $NO_3^-/NO_2^-$ Dynamics in Living cells by Fluorescence Resonance Energy Transfer (FRET) Imaging Employing a Rhizobial Two-Component Regulatory System

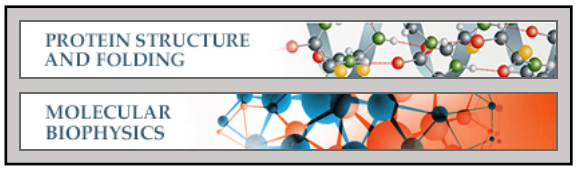


Masafumi Hidaka, Aina Gotoh, Taiki Shimizu, Kiwamu Minamisawa, Hiromi Imamura and Takafumi Uchida

*J. Biol. Chem.* published online December 2, 2015